Applied Catalysis B: Environmental 123–124 (2012) 339–350

Contents lists available at SciVerse ScienceDirect

Applied Catalysis B: Environmental

journal homepage: www.elsevier.com/locate/apcatb

# Application of spaciMS to the study of ammonia formation in lean $NO_x$ trap catalysts

Vencon Easterling[a], Yaying Ji[a], Mark Crocker[a,*], Mark Dearth[b], Robert W. McCabe[b]

[a] Center for Applied Energy Research, University of Kentucky, Lexington, KY 40511, USA
[b] Chemical Engineering Department, Ford Motor Co., Dearborn, MI 48124, USA

ARTICLE INFO

*Article history:*
Received 21 December 2011
Received in revised form 26 April 2012
Accepted 1 May 2012
Available online 10 May 2012

*Keywords:*
SpaciMS
Lean $NO_x$ trap
$NO_x$ adsorber catalyst
Storage
Reduction
Ammonia
Aging

ABSTRACT

SpaciMS was employed to understand the factors influencing the selectivity of $NO_x$ reduction in two fully formulated LNT catalysts, both degreened and thermally aged. Both catalysts contained Pt, Rh, BaO and $Al_2O_3$, while one of them also contained La-stabilized $CeO_2$. The amount of reductant required to fully regenerate each catalyst was first determined experimentally based on the OSC of the catalyst and the $NO_x$ storage capacity (NSC). In this way a correction was made for the change in catalyst OSC and NSC after aging, thereby eliminating these as factors which could affect catalyst selectivity to $NH_3$. For both catalysts, aging resulted in an elongation of the $NO_x$ storage–reduction (NSR) zone due to a decrease in the concentration of $NO_x$ storage sites per unit catalyst length. In addition to decreased lean phase $NO_x$ storage efficiency, stretching of the NSR zone affected catalyst regeneration. Three main effects were identified, the first being an increase of the $NO_x$ "puff" that appeared during the onset of the rich front as it traversed the catalyst. Spatially, $NO_x$ release tracked the NSR zone, with the result that the $NO_x$ concentration peaked closer to the rear of the aged catalysts. Hence the probability that $NO_x$ could re-adsorb downstream of the reduction front and subsequently undergo reduction by $NH_3$ (formed in the reduction front) was diminished, resulting in higher rich phase $NO_x$ slip. Second, the stretching of the NSR zone resulted in increased selectivity to $NH_3$ due to the fact that less catalyst (corresponding to the OSC-only zone downstream of the NSR zone) was available to consume $NH_3$ by either the $NH_3$-$NO_x$ SCR reaction or the $NH_3$-$O_2$ reaction. Third, the loss of OSC and $NO_x$ storage sites, along with the decreased rate of $NO_x$ diffusion to Pt/Rh sites (as a result of Pt/Rh–Ba phase segregation), led to an increase in the rate of propagation of the reductant front after aging. This in turn resulted in increased $H_2$:$NO_x$ ratios at the Pt/Rh sites and consequently increased selectivity to $NH_3$.

© 2012 Elsevier B.V. All rights reserved.

## 1. Introduction

Recent years have witnessed concerted efforts to reduce $NO_x$ emissions from mobile sources of lean exhaust gas using lean $NO_x$ trap (LNT) or selective catalytic reduction (SCR) catalysts. Although both technologies have many positive features, each approach has drawbacks which have slowed their application to the automotive marketplace. For LNT catalysts, one of the main disadvantages is the cost associated with the use of platinum group metals (PGMs), while for SCR, the cost of the injection system and refilling of the $NH_3$ source adds to the consumer's costs. However, recent studies have shown that by combining LNT and SCR catalysts in series, these drawbacks can be lessened [1–5]. In this configuration the SCR catalyst functions in a passive or in situ mode, i.e., with the storage and utilization of $NH_3$ generated by the LNT during rich purge events. Given that the presence of the SCR catalyst relaxes the $NO_x$ conversion requirements of the LNT catalyst, the volume of the LNT in the LNT–SCR system can, in principle, be lower than for an LNT-only system, thereby reducing the precious metal costs. Furthermore, the need for a urea injection system is eliminated.

To realize a LNT–SCR system capable of achieving these aims, an understanding is required of the interplay between system operating parameters and the underlying chemistry of $NO_x$ reduction. Probably the most important aspects to be considered are the generation of $NH_3$ over the LNT, and its subsequent reaction with $NO_x$ over the SCR catalyst. A potential problem in studying these processes in a LNT–SCR system is the integral nature of the catalysts. Reactants and products can react, adsorb, and desorb multiple times before exiting the system. This makes the study of LNT–SCR systems difficult using traditional laboratory techniques based on analysis of the reactor effluent.

To overcome these problems, spatially resolved capillary inlet mass spectrometry (spaciMS), developed at Oak Ridge National Laboratory, has been applied to monitor the composition of

* Corresponding author. Tel.: +1 859 257 0295; fax: +1 859 257 0302.
*E-mail address:* mark.crocker@uky.edu (M. Crocker).

0926-3373/$ – see front matter © 2012 Elsevier B.V. All rights reserved.
http://dx.doi.org/10.1016/j.apcatb.2012.05.002

simulated exhaust gas as it passes through LNT catalysts [6–14]. The key feature of a spaciMS system is the use of a capillary connected to the sample cell of a mass spectrometer. The capillary allows the internal gas stream to be analyzed at different points along the length of the LNT or SCR catalyst under study. Consequently, the gaseous components present can be monitored on both a spatial and temporal scale. Partridge et al. employed spaciMS to study $NH_3$ formation and utilization over a $Pt/Ba/Al_2O_3$ catalyst during regeneration with $H_2$ [10]. It was found that $NH_3$ was formed at the same time as the $N_2$ product inside the catalyst during regeneration, and was consumed as aggressively as the $H_2$ reductant along the catalyst. From this it was concluded that the intermediate $NH_3$ regeneration pathway plays an important role in LNT catalyst regeneration. The same research group also utilized this technique to study the effect of sulfur on the spatiotemporal distribution of $NO_x$ storage and reduction [11]. Prior to sulfation, $NO_x$ storage/reduction was found to be localized in the front portion of catalyst, whereas sulfation resulted in a shift of the $NO_x$ storage/reduction (NSR) zone downstream, thereby decreasing the length of the downstream zone in which only oxygen was stored. These workers also reported an increase in selectivity to $NH_3$ after sulfation, and ascribed it to decreased oxidation of $NH_3$ slipping from the NSR zone by the oxygen stored downstream [11,12]. A more recent study by this group further demonstrated that $NH_3$ slip at the catalyst exit increased with sulfur loading due to its formation closer to the catalyst outlet and decreased $NH_3$ conversion by stored oxygen downstream of the NSR zone [13]. Moreover, during catalyst regeneration the extent of $NO_x$ readsorption downstream of the NSR zone was found to diminish after sulfation, resulting in earlier and broader $NO_x$ peaks at the catalyst outlet. The spaciMS technique was also applied in another recent LNT study by Luo et al. [14] in which catalyst desulfation was examined. For a partially sulfated commercial catalyst, the plug-like sulfur profile was redistributed after desulfation at 600 °C as a result of re-adsorption. The extent of re-adsorption was found to be determined by the catalyst formulation and sulfation degree.

We have previously investigated the effect of regeneration conditions on $NH_3$ formation in LNT catalysts [15]. One of the findings from these studies was that $NH_3$ selectivity is dependent on the local $H_2$:$NO_x$ ratio at the precious metal sites. Increasing the regeneration time or reductant concentration fed to the catalyst increases this ratio and thereby increases the amount of $NH_3$ formed, as opposed to $N_2$. Conversely, increasing the amount of $NO_x$ stored decreases the selectivity to $NH_3$. It was also observed that the addition of a ceria-based oxygen storage material to a $Pt/Rh/BaO/Al_2O_3$ catalyst caused a decrease in $NH_3$ selectivity [15–18], which was explained on the basis that consumption of reductant by stored oxygen results in decreased $H_2$:$NO_x$ ratios during regeneration, which favors the formation of $N_2$ over $NH_3$. In addition, oxygen stored in the rear of the catalyst can consume $NH_3$ formed upstream via oxidation to produce $N_2$, NO, or $N_2O$. After aging, increased selectivity to $NH_3$ was observed, for both the ceria-containing and ceria-free catalyst. In principle, this increase in selectivity to $NH_3$ can be accounted for by any one of a number of factors [15]:

(i) Aging-induced Pt sintering, resulting in Pt–Ba phase segregation. Consequently, the rate of $NO_x$ transport to the Pt sites during regeneration is decreased. As Harold and co-workers have pointed out [19], if this rate is slower than the $H_2$ feed rate, then $H_2$ will break through with substantially more $NO_x$ remaining on the catalyst. Consequently, the Pt surface will be predominantly covered by hydrogen, and as the stored $NO_x$ diffuses to the Pt particles, $NH_3$ will be formed with high selectivity. Modeling studies confirm this idea, i.e., that $NH_3$ formation is favored when solid-phase diffusion of $NO_x$ to the Pt/Ba interface is the rate determining process, which becomes increasingly likely as the Pt dispersion decreases [20].

(ii) For a fixed concentration of reductant, the decreased oxygen storage capacity (OSC) of the aged catalysts should result in higher effective $H_2$:$NO_x$ ratios in the reduction front due to decreased reductant consumption by stored oxygen, thereby favoring $NH_3$ formation. Furthermore, there is less oxygen available downstream of the reductant front to react with formed $NH_3$.

(iii) After aging, there are fewer $NO_x$ storage sites available per unit of catalyst length. This should result in higher effective $H_2$:$NO_x$ ratios in the reductant front, again favoring $NH_3$ formation [15].

(iv) The length of the $NO_x$ storage–reduction zone increases due to the decrease in $NO_x$ storage capacity (NSC) as the catalyst ages [11,12,15]. More $NH_3$ slips from the LNT without being oxidized because the increased length of the NSR zone decreases the length of the downstream OSC-only zone.

(v) After aging, higher $NH_3$ emissions may result from decreases in the rates of $NH_3$ consumption via reaction with $NO_x$ or $O_2$ stored downstream of the reaction front.

From the foregoing, it is evident that $NH_3$ selectivity after aging is likely to be dependent – at least in part – on the residual OSC of the catalyst, as well as the amount of $NO_x$ stored. In an effort to distinguish between the factors that can account for increased LNT selectivity to $NH_3$ after aging, in this study we adjusted the amount of reductant used to regenerate each catalyst (degreened and thermally aged) based on the OSC of the catalyst and the $NO_x$ storage capacity (NSC). In this way we attempted to correct for the change in catalyst OSC and NSC after aging, thereby eliminating these as factors. SpaciMS was used to monitor the $NO_x$ storage and reduction processes for degreened and aged catalysts in order to investigate the contribution of other factors to $NO_x$ reduction selectivity.

**Table 1**
Composition of catalysts used in this study.

| Component | Catalyst code/nominal loading | |
|---|---|---|
| | B-225 | BC-175 |
| Pt (g/L) | 3.05 | 2.38 |
| Rh (g/L) | 0.61 | 0.48 |
| BaO[a] (g/L) | 26 | 20 |
| $CeO_2$[b] (g/L) | 0 | 67 |
| $\gamma$-$Al_2O_3$[c] (g/L) | Balance | Balance |
| Total washcoat (g/L) | 225 | 175 |

[a] 21.5 wt% supported on $\gamma$-$Al_2O_3$.
[b] Stabilized with 5 wt% $La_2O_3$.
[c] Stabilized with 3 wt% $La_2O_3$.

## 2. Experimental

### 2.1. Catalyst preparation

Two fully formulated Ba-based LNT catalysts were used in this study, the compositions of which are shown in Table 1. For simplicity, the BaO-only formulation is denoted as B-225 (where 225 refers to the washcoat loading in g/L), while the catalyst containing both BaO and $CeO_2$ is denoted as BC-175 (containing a washcoat loading of 175 g/L). Details of the catalyst preparation have been described elsewhere [16,17]. In both cases, the washcoat was applied to a 4 in. × 6 in. cordierite monolith substrate, possessing a cell density of 400 cpsi and a wall thickness of 6.5 mil. The BaO component (21.5 wt %) was supported on $\gamma$-alumina, while bare alumina was also used as a balance to bring the total washcoat loadings to the values indicated in Table 1.

### 2.2. Catalyst aging

A 1.75 cm × 2.54 cm ($d \times l$) core was drilled out from the LNT monolith and was wrapped with ceramic fiber and positioned in a quartz tube. Degreening the catalyst consisted of exposing the catalyst to neutral conditions (5% $CO_2$, 5% $H_2O$, balance $N_2$) at 800 °C for 2 h. Aging the catalyst involved subjecting the catalyst to continuous lean conditions (8% $O_2$, 5% $CO_2$, 5% $H_2O$, and balance $N_2$) at 800 °C for 24 h. In both cases, the gas flow was adjusted to give a GHSV of 30,000 $h^{-1}$.

### 2.3. Catalyst characterization

#### 2.3.1. $N_2$ physisorption

Surface area and pore volume analysis was performed according to the BET method by nitrogen adsorption at −196 °C using a Micromeritics Tri-Star system. Prior to the measurements catalyst samples (washcoat and monolith) were ground to a fine powder and outgassed overnight at 160 °C under vacuum.

#### 2.3.2. Pulsed $H_2$ chemisorption

The dispersion of precious metal (Pt + Rh) was determined with a Micromeritics AutoChem II Analyzer by means of pulsed $H_2$ chemisorption at dry ice temperature (−78 °C). This temperature was chosen in an effort to minimize H spillover from the metal to the support material [21]. 1 g of sample (as a fine powder), including both washcoat and substrate, was loaded into the reactor. After being oxidized at 400 °C in 10% $O_2$/He for 15 min, followed by reduction at 300 °C in 10% $H_2$/Ar for 15 min, the catalyst was heated to 400 °C (hold time 10 min) in flowing Ar to remove adsorbed H. Pulsed $H_2$ chemisorption was initiated using a four-way valve after the catalyst had been cooled to −78 °C. During this measurement, 0.5 mL of 10% $H_2$/Ar was pulsed into the reactor every 2 min, the $H_2$ signal at the reactor outlet being monitored with a thermal conductivity detector (TCD). $H_2$ pulsing was terminated after the TCD signal had reached a constant value, i.e., the total precious metal (Pt + Rh) sites were saturated with $H_2$. Assuming a 1:1 ratio of atomic hydrogen to surface Pt or Rh, the metal dispersion was calculated based on the amount of H adsorbed.

### 2.4. SpaciMS measurements

#### 2.4.1. Determination of the amount of reductant required for catalyst regeneration

Determination of the amount of reductant required for catalyst regeneration was based on the catalyst oxygen storage capacity (OSC) and the amount of $NO_x$ stored during lean–rich cycling. Hydrogen was measured using a V & F Airsense H-sense mass spectrometer. All other species, i.e., NO, $NO_2$, $O_2$, $H_2O$, and $NH_3$, were measured using a V & F Airsense 2000 mass spectrometer using the low energy source, Hg, as the ion source; this enabled these species to be tracked individually, without interference from other species present. The mass spectrometer had been modified for spaciMS measurements by incorporating a 0.37 mm outer diameter (0.18 mm i.d.) stainless steel capillary connected to the sample chamber. The sampling rate was 14 sccm and data were collected at 3 Hz. After the spaciMS was calibrated, the sample was purged by heating it to 450 °C under a 4.2% $H_2$ in $N_2$ flow until the $NH_3$ concentration measured by the spaciMS fell to below 4 ppm at a position 1 mm from the rear of the catalyst. Once this level was achieved, the reactor temperature was dropped to the desired temperature (200 °C, 250 °C, or 300 °C) and the samples were exposed to 60 s lean/5 s rich cycles. The lean phase gas contained 8% $O_2$, 5% $CO_2$, 5% $H_2O$, and balance $N_2$, while the rich phase gas contained 4.2% $H_2$, 5% $CO_2$, 5% $H_2O$, and balance $N_2$. After 5 cycles the flow was switched from the outlet of the reactor to the reactor bypass so that the baseline hydrogen level could be measured. The OSC was determined by subtracting the cycle-averaged outlet $H_2$ concentration from the inlet $H_2$ concentration.

In separate experiments, the $NO_x$ storage capacity of the LNT was determined. The feed was switched to neutral conditions (5% $CO_2$, 5% $H_2O$, and balance $N_2$), and once equilibrated, the catalyst was subjected to lean conditions for 60 s, using a feed consisting of 300 ppm NO, 8% $O_2$, 5% $CO_2$, 5% $H_2O$, and balance $N_2$. Simultaneously, the outlet $NO_x$ concentration was monitored by the spaciMS probe at a position 1 mm from the rear catalyst face. At the end of the lean 60 s period, the spaciMS probe was moved to a position 4 cm in front of the catalyst and the measurement was repeated. The difference between the two integrated $NO_x$ concentrations gave the amount of $NO_x$ stored. The amount of reductant required for LNT regeneration was then calculated from the sum of the measured OSC and 2.5 times the value of the $NO_x$ storage measurement. This factor of 2.5 represents the stoichiometry of $NO_x$ reduction by $H_2$ to give $N_2$ (assuming that $NO_x$ is stored as nitrate) as reported in the literature [22,23]:

$$Ba(NO_3)_2 + 8H_2 \rightarrow 2NH_3 + Ba(OH)_2 + 4H_2O \quad (1)$$

$$3Ba(NO_3)_2 + 10NH_3 \rightarrow 8N_2 + 3Ba(OH)_2 + 12H_2O \quad (2)$$

The sum of reactions (1) and (2) leads to the overall stoichiometry for the reduction of Ba nitrate by $H_2$:

$$Ba(NO_3)_2 + 5H_2 \rightarrow N_2 + Ba(OH)_2 + 4H_2O \quad (3)$$

#### 2.4.2. $NO_x$ storage and reduction measurements

With the required reductant amounts having been determined for each catalyst (both degreened and aged) at 200, 250, and 300 °C, $NO_x$ storage and reduction measurements were performed at these temperatures during 60 s lean/5 s rich cycles. The lean phase gas contained 300 ppm NO, 8% $O_2$, 5% $CO_2$, 5% $H_2O$, and balance $N_2$, while the rich phase gas contained the calculated amount of $H_2$ for each catalyst, 5% $CO_2$, 5% $H_2O$, and balance $N_2$. Prior to the measurements, each sample was exposed to the cycling conditions until the component concentrations in the reactor effluent were constant from one cycle to the next. Once "stationary" cycles had been attained (∼1 h), data pertaining to the concentrations of NO, $NO_2$, $O_2$, $H_2O$ and $NH_3$ were collected at different positions using spaciMS. The first of these positions corresponded to the rear face of the catalyst (25.4 mm from the catalyst inlet), with successive sampling at, 16.4 mm, 8.4 mm, 4.4 mm, and the front face (0 mm from the inlet). By sampling in this manner (from rear to front), the chances of contaminating the capillary with particles from the washcoat of the catalyst were lessened. Note that the "0 mm" position actually corresponds to a position of 0.1 mm; this was done in order to ensure that the capillary was correctly aligned with the selected channel. Consequently, when feeding NO in the lean phase, some $NO_2$ (corresponding to ca. 15% NO conversion) was detected at the 0.1 mm position, arising from a combination of catalyzed NO oxidation in the first 0.1 mm of the catalyst and gas phase NO oxidation in the feed lines. For each position, the system was allowed to stabilize for two 60 s/5 s cycles before data were taken over five successive cycles. These cycles were then averaged to produce the spatio-temporal plots of species concentration versus time for each axial location.

$NO_x$ storage efficiency (NSE) is defined in this study as:

$$\frac{\text{Inlet concentration of } NO_x - \text{Concentration of } NO_x \text{ at measurement location}}{\text{Inlet concentration of } NO_x} \times 100\% \quad (4)$$

Rich phase $NO_x$ release is defined as:

$$\frac{\text{Concentration of rich phase } NO_x \text{ release at measurement location}}{\text{Inlet lean concentration of } NO_x - \text{Outlet lean concentration of } NO_x} \times 100\% \quad (5)$$

**Table 2**
Physical properties of degreened and aged catalysts.

| Catalyst | Total BET surface area ($m^2/g$)[a] | | Pore volume ($cm^3/g$)[a] | | Average pore radius (nm)[a] | | PGM dispersion (%) | |
|---|---|---|---|---|---|---|---|---|
| | Degreened | Aged | Degreened | Aged | Degreened | Aged | Degreened | Aged |
| B-225 | 41.1 | 35.4 | 0.148 | 0.137 | 7.19 | 7.72 | 21.6 | 5.4 |
| BC-175 | 26.3 | 25.4 | 0.105 | 0.109 | 7.96 | 8.56 | 9.8 | 2.5 |

[a] Includes cordierite monolith.

In both Eqs. (4) and (5), all concentrations are cycle-averaged integrated values (ppm s).

## 3. Results

### 3.1. Catalyst characterization

The results of $N_2$ physisorption and $H_2$ chemisorption measurements performed on the degreened and aged catalysts are collected in Table 2. Both catalysts displayed a small loss in surface area after aging, which for the B-225 sample was accompanied by a decrease in the pore volume. Sintering of the catalyst is evidenced by an increase in the average pore radius, which can be attributed to collapse of the smaller pores during aging. Comparing the PGM dispersions derived from $H_2$ chemisorption measurements, it is evident that exposure of the catalysts to high temperatures during aging resulted in significant PGM sintering. Indeed, for both catalysts, a decrease in PGM dispersion of ca. 75% was seen. These results are consistent with the degree of Pt sintering observed in a previous study in which model LNT catalysts were likewise subjected to continuous lean conditions at 800 °C for periods of up to 16 h [24].

### 3.2. Amount of reductant required for complete $NO_x$ reduction during rich purging

The minimum amount of reductant required to fully regenerate a LNT during lean–rich cycling can be determined from the oxygen storage capacity (OSC) and the $NO_x$ storage capacity (NSC). In this study, the $H_2$ concentration during lean–rich cycling was adjusted so that the degreened and aged catalysts would be exposed to a stoichiometric quantity of $H_2$ with respect to complete regeneration. This adjustment allows for a sounder basis when comparing fresh and aged catalysts in terms of the selectivity of $NO_x$ reduction, given that excess reductant would influence the selectivity towards $NH_3$ production. The results from these OSC and NSC measurements, performed on catalysts B-225 and BC-175, are shown in Fig. 1. The column chart is arranged such that the data for the non-ceria-containing catalyst B-225 are shown on the left half of the figure, while data for the ceria-containing catalyst are on the right. Each of the stacked columns shows the amount of $H_2$ required to consume the oxygen stored on the catalyst and to reduce the stored $NO_x$. The fact that $H_2$ concentrations required for complete regeneration of BC-175 are greater than those for B-225 can be attributed to the presence of La-stabilized $CeO_2$ in BC-175. Comparing the OSC and NSC with temperature, it is apparent that for both the B-225 and BC-175 catalysts the measured values increase with temperature. This trend is expected for BC-175 since $CeO_2$ has increased OSC at higher temperatures due to the increased concentration of oxygen defect sites [25]. In addition, the NSC of Ba-based catalysts increases with temperature for the temperature range studied here [16,17].

Considering the aged catalysts, an obvious trend is that the amount of reductant required for catalyst regeneration decreases after aging due to decreases in OSC and NSC. During aging, Pt sintering occurs, leading to a decrease in the Pt–Ba interfacial perimeter

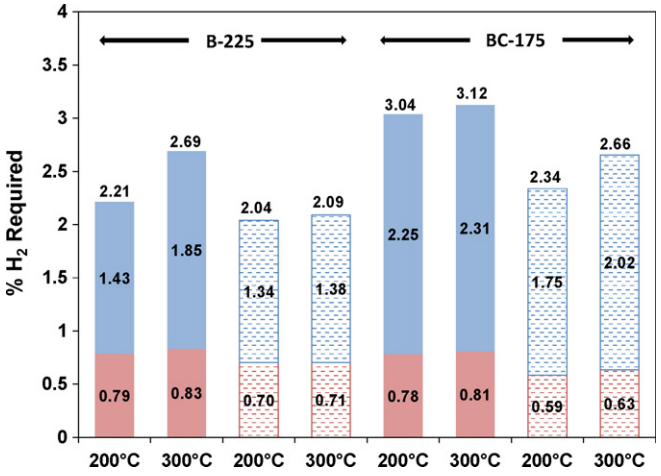


**Fig. 1.** Required amount of $H_2$ during 60 s lean−5 s rich cycling for catalyst regeneration. Solid colors represent values for degreened catalysts and patterned colors represent values for aged catalysts. The blue or top values in the columns represent the oxygen storage capacities, and the red or bottom values represent the $NO_x$ storage capacities. (For interpretation of the references to color in this figure legend, the reader is referred to the web version of this article.)

[16,20], i.e., phase segregation occurs between the Pt and Ba storage sites [26–31]. Consequently, for a given length of catalyst, fewer storage sites are present and less reductant is needed. Additionally, agglomeration of the Pt during aging reduces the number of sites available for oxygen adsorption during lean conditions. Finally, in the case of BC-175, a significant portion of the decrease in OSC can be attributed to the loss of oxygen defect sites in the structure of the La-stabilized $CeO_2$ component after aging. Mamontov et al. [25] have shown that OSC correlates with defect site concentration rather than surface area, the latter being relatively unchanged after aging based on the negligible change in total catalyst surface area (Table 2). Indeed, in their work Mamontov and co-workers found that significant decrease of OSC occurred upon aging a ceria sample at 800 °C. In addition, some contribution to the loss in OSC may come from the sintering of Pt supported on the $CeO_2$ component, given that Pt acts essentially as a conduit for oxygen storage and release.

### 3.3. Non-ceria containing catalyst

#### 3.3.1. $NO_x$ storage

Once the amounts of reductant required for catalyst regeneration were determined, the catalysts were subjected to $NO_x$ storage–reduction experiments. The non-ceria containing sample was subjected to 60/5 s cycles and evaluated at three temperatures: 200 °C, 250 °C, and 300 °C. Data pertaining to the measured lean $NO_x$ storage efficiencies (NSEs) are shown in Fig. 2. For degreened catalyst B-225 the NSE increases along the length of the catalyst (at all temperatures), while NSE also increases with temperature in the range studied. Maximum NSE values are reached around the midpoint of the catalyst, providing an indication of the length of the $NO_x$ storage zone under these experimental conditions.

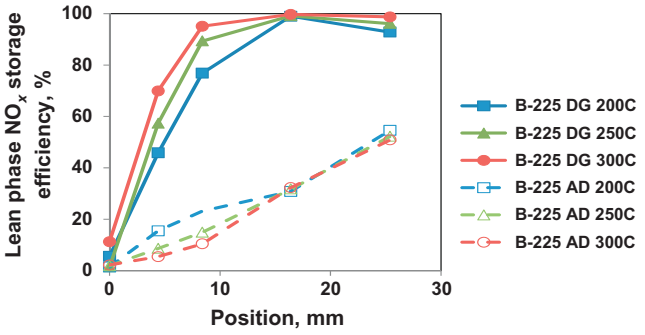


**Fig. 2.** Lean $NO_x$ storage efficiency as a function of position for degreened (DG) and aged (AD) catalyst B-225.

Additional detail is provided in Fig. 3a and b, in which the cycle-averaged NO and $NO_2$ concentrations are plotted at each measurement point along the length of the catalyst. For the degreened catalyst, a rapid decrease in the NO concentration begins at 4.4 mm, the NO concentration reaching zero by the 16.4 mm position. At this juncture, an explanation is required for the slight increase in NO and $NO_2$ concentrations observed in moving from 16.4 to 25.4 mm positions in Fig. 3. As noted by Partridge and Choi [10], the spaciMS system is capable of great sensitivity. This, combined with possible over-sampling at the rear of the catalyst (due to the high sampling rate and sampling position) can lead to the capillary sampling gas slightly beyond the rear of the catalyst. At this location the gas is comprised of the effluent from all of the channels in the catalyst. Bearing in mind that not all of the channels in the catalyst will have exactly the same amount of washcoat, the concentration of $NO_x$ just outside the rear of the catalyst can be different compared to the channel in which the capillary is located. Furthermore, the outer diameter of the capillary used in these experiments (0.37 mm) was significant compared to the channel

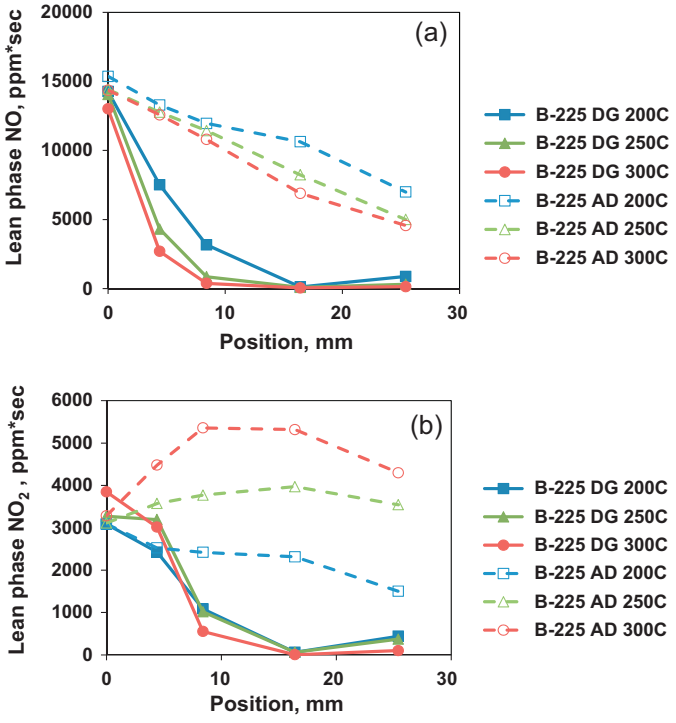


**Fig. 3.** (a) Lean phase NO concentration and (b) lean phase $NO_2$ concentration as a function of position during $NO_x$ storage on degreened (DG) and aged (AD) catalyst B-225.

width (1.1 mm). The resulting restriction of the gas flow in the channel may result in a slightly different residence time, and hence gas composition, compared to the surrounding channels.

From Fig. 3a it is evident that the amount of NO present at each position increases with decreasing temperature. Conversely, the $NO_2$ concentrations increase with increasing temperature in the range of 200–300 °C. These results are consistent with an increase in the rate of oxidation of NO to $NO_2$ with increasing temperature. At 300 °C, the rate of $NO_2$ formation is fast relative to the linear gas velocity and $NO_2$ is stored in the front of the catalyst. At the lowest temperature, 200 °C, the slower rate of oxidation of NO results in the feed gas traveling further along the length of catalyst before $NO_2$ is generated and then stored. Consequently, more of the catalyst is used for $NO_x$ storage. This finding is consistent with a previous report that the length of the NSR zone decreases with increasing temperature [11]. In addition, at lower temperatures, a portion of the $NO_x$ can be stored as $Ba(NO_2)_2$, although the literature suggests that this pathway is fairly minor. For example, under their experimental conditions Forzatti and co-workers [4] found that at 200 °C ca. 20% of $NO_x$ was stored as $Ba(NO_2)_2$ and 80% was stored as $Ba(NO_3)_2$. Fig. 4 provides a schematic of the $NO_x$ storage process and depicts the relative NO and $NO_2$ concentrations measured at 200 °C along the length of the catalyst.

Fig. 2 also contains the NSE results for the aged B-225 catalyst. In contrast to the data for the degreened catalyst, the NSE does not reach a maximum value within the length of the catalyst, indicating that the whole of the catalyst is used for $NO_x$ storage. Indeed, the maximum NSE after aging does not exceed 60% at any measurement temperature. Hence, the OSC-only zone in the schematic shown in Fig. 4 (which corresponds to zone 2) is effectively eliminated after aging. NSEs at the three temperatures are very similar, although because the data point at the 8.4 mm position in Fig. 2 is not available, the NSE at 200 °C appears to be greater than at 250 or 300 °C. This is largely a consequence of the missing point, given that at all of the other measurement points the values at each of the temperatures are very similar.

From Fig. 3a, it is evident that the NO concentrations measured for the aged sample decrease gradually compared to the degreened case, NO being present in significant concentrations throughout the entire length of the catalyst. As shown in Fig. 3b, the $NO_2$ concentrations increase along the catalyst before reaching a maximum and then decreasing. A comparison between the data collected for the degreened and aged catalyst at 200 °C is shown in Fig. 4. The increase in measured NO and $NO_2$ concentrations for the aged sample can be explained on the basis that the concentration of $NO_x$ storage sites is decreased after aging. Due to sintering of the Pt particles, the distance between Pt and Ba is increased, thereby necessitating that the $NO_2$ formed on Pt has to diffuse a greater distance to reach the Ba storage sites as compared to the degreened catalyst. This results in an effective decrease in the number of fast $NO_x$ storage sites with the consequence that $NO_2$ tends to travel downstream of the NO oxidation sites before eventually being stored. At the same time, it is evident that the NO oxidation function of the catalyst is degraded after aging. As noted above, the NO concentration decreases quite slowly along the length of the catalyst, whereas, a sharp drop-off in NO concentration is depicted in Fig. 3a for the degreened B-225 catalyst. This indicates that aging results in both a loss of NO oxidation sites and $NO_2$ storage sites relative to the degreened sample.

### 3.3.2. $NO_x$ reduction

During $NO_x$ reduction experiments, the rich phase of the 60/5 s cycles contained a concentration of $H_2$ determined from the OSC/NSC study shown in Fig. 1, along with 5% $CO_2$, 5% $H_2O$, and balance $N_2$. The resulting cycle-averaged $NO_x$ conversions are collected in Table 3. In general, cycle-averaged $NO_x$ conversion in

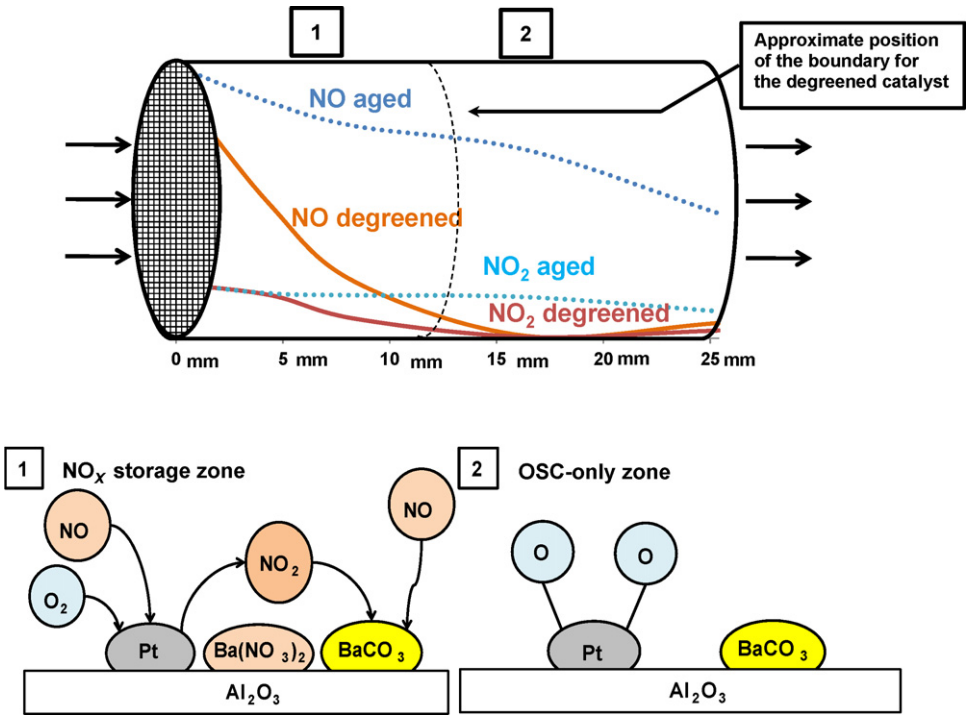


**Fig. 4.** Schematic showing NO and $NO_2$ concentrations along the length of the catalyst and the mechanism of $NO_x$ storage under lean conditions. Note that the relative concentrations depicted correspond to actual data collected at 200 °C for catalyst B-225.

lean–rich cycling experiments show a strong correlation with $NO_x$ storage efficiencies [16]. Comparing the cycle-averaged conversions in Table 3 with the lean NSE values shown in Fig. 2, a larger discrepancy is seen between the two values at 200 °C, as compared to 300 °C (see Supplementary Data, Fig. SD1). The source of this difference can be attributed to the $NO_x$ "puff" that occurs at the beginning of the transition from lean to rich conditions. Data pertaining to the "puff" are depicted graphically in Fig. 5. For the degreened B-225 catalyst, the amount of rich $NO_x$ release decreases at 250 °C and 300 °C along the entire length of the catalyst, indicating that it is re-adsorbed and subsequently reduced. In contrast, at 200 °C the rich $NO_x$ release increases along the length of the catalyst until 8.4 mm from the front of the catalyst and then decreases. This increased amount of $NO_x$ measured during the rich phase at 200 °C (and indeed emitted from the catalyst) can be explained on the basis that (i) $NO_x$ storage and release is moved further along the length of the catalyst at low temperatures [11,12], and (ii) the rich phase $NO_x$ release is greater at low temperatures due to the imbalance in the rates of $NO_x$ release and $NO_x$ reduction [16,17], i.e., a fraction of the $NO_x$ is rapidly released into the product stream but is not fully consumed by $H_2$.

Selectivity to $NH_3$ as a function of the sampling position in the catalyst is shown in Table 3 and Fig. 6. Note that in this work $N_2O$, the other possible $NO_x$ reduction product along with $N_2$ and $NH_3$, was not monitored. $N_2O$ formation over the catalysts used in this study was examined separately and will be the subject of a future report. For the degreened B-225 catalyst the $NH_3$ selectivity first increases from the front face of the catalyst, reaches a maximum close to the end of the $NO_x$ storage zone, and then decreases. In order to explain these findings, it is necessary to consider the

**Table 3**
Comparison of cycle-averaged $NO_x$ conversion and $NH_3$ selectivity during lean–rich cycling for degreened and aged catalysts.

| Catalyst | Temperature (°C) | Position (mm) | Cycle-averaged $NO_x$ conversion (%) | | $NH_3$ selectivity (%) | |
|---|---|---|---|---|---|---|
| | | | Degreened | Aged | Degreened | Aged |
| B-225 | 200 | 4.4 | 43.6 | 13.6 | 6.4 | 2.4 |
| | | 8.4 | 73.4 | –[a] | 9.8 | –[a] |
| | | 16.4 | 98.7 | 27.2 | 4.3 | 7.5 |
| | | 25.4 | 91.6 | 49.8 | 2.6 | 11.1 |
| | 300 | 4.4 | 69.0 | 4.7 | 9.3 | 0.8 |
| | | 8.4 | 94.6 | 9.3 | 5.9 | 3.0 |
| | | 16.4 | 99.7 | 30.0 | 0.4 | 11.9 |
| | | 25.4 | 98.6 | 48.6 | 1.0 | 21.4 |
| BC-175 | 200 | 4.4 | 9.8 | 7.6 | 6.1 | 1.0 |
| | | 8.4 | 29.6 | 28.2 | 29.4 | 34.2 |
| | | 16.4 | 55.4 | 54.4 | 56.2 | 60.4 |
| | | 25.4 | 77.0 | 88.8 | 45.1 | 72.2 |
| | 300 | 4.4 | 22.7 | 8.1 | 3.7 | 1.6 |
| | | 8.4 | 53.3 | 23.3 | 9.4 | 6.9 |
| | | 16.4 | 86.8 | 56.0 | 8.6 | 15.2 |
| | | 25.4 | 98.6 | 66.5 | 0.9 | 14.9 |

[a] Data not available for this position.

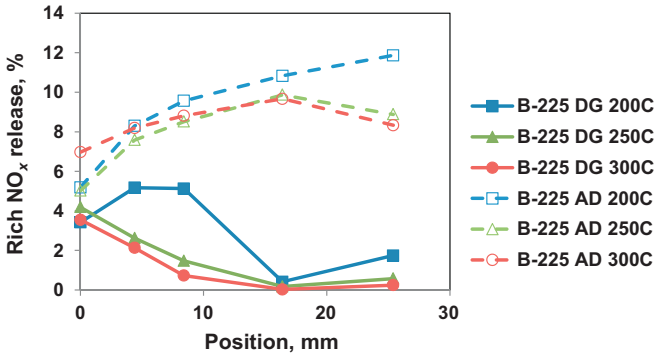


**Fig. 5.** Rich phase $NO_x$ release as a function of position during regeneration of degreened (DG) and aged (AD) catalyst B-225.

reductant front as it moves along the axial length of the catalyst. According to the model proposed by Ribeiro and co-workers [32,33] and others [10,23,34,35], during LNT regeneration a $H_2$-rich reaction front propagates along the length of the catalyst in which $N_2$ and $NH_3$ are formed from the reduction of the stored $NO_x$. The formed $NH_3$ may then react further with nitrates stored downstream of the front, resulting in the formation of $N_2$. This explains the temporal sequence of product formation, $N_2$ breakthrough occurring before $NH_3$. Breakthrough of the $NH_3$ corresponds to the point at which the stored $NO_x$ and $O_2$ are sufficiently depleted for the $NH_3$ consumption to be incomplete.

During regeneration, a number of zones effectively exist in the catalyst (see Fig. 7) [11–13,34–36]. Upstream of the reductant front (zone 1), hydrogen has already consumed oxygen present on the Pt sites and depending on the temperature (vide infra), may or may not have reduced all of the stored $NO_x$. The ratio of $H_2$ to residual $NO_x$ (if present) is high (given that the reduction front has already moved downstream), and hence $NH_3$ formation is favored. In the reductant front (zones 2 and 3), $NH_3$ is both generated and consumed. Downstream of the front (zone 4), $NO_x$ and adsorbed oxygen are present. The significance of this is that $NH_3$ produced in or behind the front can be consumed in the $NO_x$-$NH_3$ SCR or $NH_3$-$O_2$ reactions. Zone 5 corresponds to the OSC-only zone, i.e., the region downstream of the NSR zone.

Given that at moderate to high temperatures $NO_x$ reduction displays the characteristics of a feed-limited process [32,33,35], significant $NO_x$ reduction behind the reduction front is not expected in this temperature range, i.e., stored $NO_x$ should be fully consumed in the reduction front. However, Clayton et al. [35] have observed that at lower temperatures (<230 °C) $H_2$ and $NH_3$ break through well before all of the stored $NO_x$ has reacted, the implication being that catalyst regeneration is limited by chemical processes at the Pt/Ba interface. This explains why catalyst selectivity to $NH_3$ increases

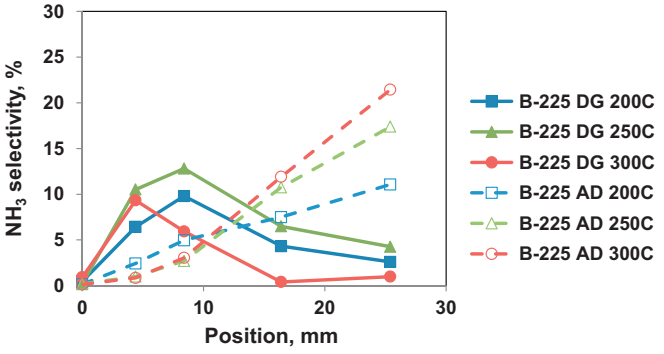


**Fig. 6.** Rich phase $NH_3$ selectivity as a function of position for degreened (DG) and aged (AD) catalyst B-225.

significantly with decreasing temperature, as illustrated by the data in Table 3. Modeling studies by the same group [20] have confirmed that $NH_3$ generation is favored under conditions when $NO_x$ transport to the Pt/Ba interface is the rate determining process. A contributing factor to the increased $NH_3$ selectivity observed at low temperatures can be the slow kinetics of the $NO_x$-$NH_3$ SCR reaction [23]. However, several studies employing catalysts and conditions similar to those employed in the present work have shown that the SCR reaction typically lights off below 200 °C [23,35,37,38]; hence, this is not a factor in the case of degreened catalyst B-225.

Aging at 800 °C significantly affects the performance of the B-225 catalyst, as shown by the greatly decreased cycle-averaged $NO_x$ conversions reported in Table 3. As shown, the $NO_x$ conversions measured at 200 and 300 °C reach a maximum at the outlet of the catalyst (25.4 mm), reflecting the lengthening of the NSR zone after aging. This latter point is clearly apparent in Fig. 5, which shows that the rich phase $NO_x$ release increases over the length of the catalyst rather than peaking within the first 8.4 mm (as seen for the degreened catalyst). The total amount of $NO_x$ release is also greater than for the degreened sample. Higher $NO_x$ release at 0.0 mm is explained by an increase in the imbalance of $NO_x$ release and reduction rates. Aging results in sintering of the PGM sites and consequently the rate of reduction of $NO_x$ by adsorbed hydrogen at these sites is slower [39]. Furthermore, for a given length of catalyst, there are now fewer sites located downstream for the $NO_x$ in the gas phase to re-adsorb on the catalyst. This is due to the stretching of the $NO_x$ storage zone, i.e., the storage sites downstream have already been filled.

As shown in Table 3 and Fig. 6, the selectivity to $NH_3$ continues to increase to the end of the aged catalyst sample. For the degreened sample maximum $NH_3$ release is seen towards the end of the $NO_x$ storage zone; given that the NSR zone now encompasses the entire length of the sample, it follows that $NH_3$ selectivity reaches a maximum towards the rear of the sample. Indeed, as shown in Fig. 7, for the degreened sample both the $NH_3$ and NO concentrations reach a maximum within the first 10 mm of the catalyst, whereas these concentrations continue to increase along the length of the catalyst for the aged sample. For the aged catalyst, two additional effects must be considered. First, stretching of the storage–reduction zone results in the elimination of the downstream OSC-only zone. Therefore, the $NH_3$ that is formed is less likely to be consumed by adsorbed oxygen downstream of the reduction front. Second, as discussed in Section 1, segregation of the Pt and Ba phases during aging results in a decrease in the rate of $NO_x$ transport (reverse spillover) to the Pt sites. Consequently, the Pt surface will be predominantly covered by hydrogen, and as the stored $NO_x$ diffuses to the Pt particles, $NH_3$ will be preferentially formed.

Analysis of the temporal data provides additional insights. In Fig. 8a and b, $NH_3$ concentrations are plotted versus time at each sampling position for the degreened and aged catalysts, respectively. Note that in the plots, the feed gas was switched from lean to rich at 31 s. Examining the data for the degreened catalyst in Fig. 8a, the $NH_3$ concentration increases from the front of the catalyst until the midpoint of the catalyst (between the 8.4 mm and 16.4 mm positions). Furthermore, a delay is present in the appearance of $NH_3$ from one sampling position to the next over the length of the catalyst. For example, at the 4.4 mm position, a ~1 s delay from the onset of rich conditions to the appearance of $NH_3$ exists, with additional delays at each of the subsequent measurement points. This finding is consistent with previous reports [10,35] and is evident that significant $H_2$ consumption precedes $NH_3$ formation, i.e., due to the reaction of $H_2$ with stored oxygen and with stored $NO_x$ to generate $N_2$. The decrease in $NH_3$ concentration that begins between the 8.4 mm and 16.4 mm positions and continues until the rear of

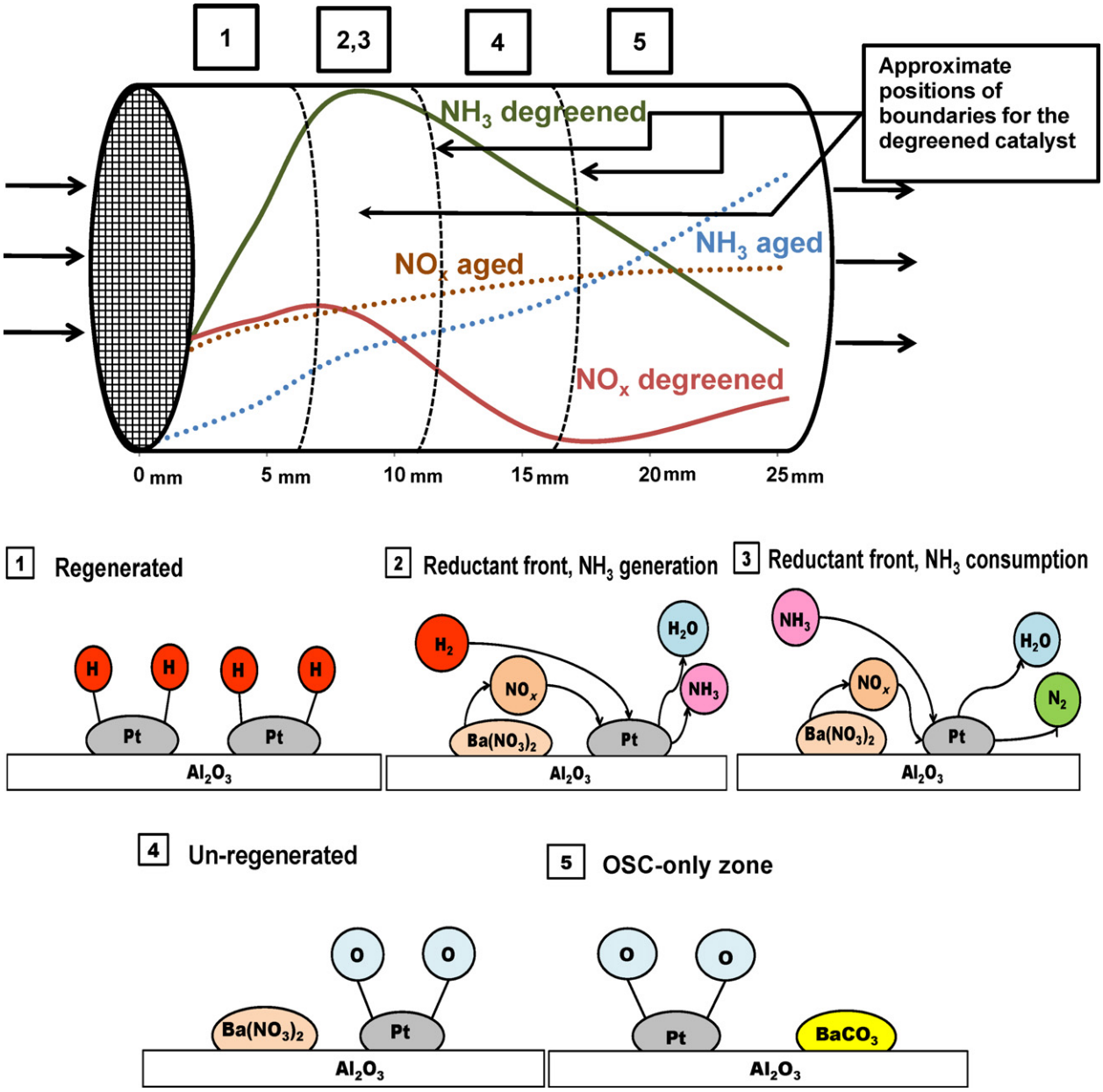


**Fig. 7.** Schematic showing $NO_x$ and $NH_3$ concentrations along the length of the catalyst and the mechanism of $NO_x$ reduction under rich conditions (after Pihl et al. [36]). Note that the relative concentrations depicted correspond to actual data collected at 200 °C for catalyst B-225.

catalyst demonstrates that some of the $NH_3$ is being consumed before reaching the end of the catalyst.

Comparing these results with the data for the aged catalyst, a clear difference is the lack of delay between the appearance of $NH_3$ at each measurement point in the aged catalyst. Indeed, as shown in Fig. 8b, the initiation of $NH_3$ release at the different sampling locations occurs almost simultaneously for the aged sample. These observations clearly indicate that the reductant front propagates more rapidly along the length of the aged catalyst than the degreened sample. This increase in the velocity of the front can be attributed in part to the lower amounts of $NO_x$ and $O_2$ stored in the front of the catalyst. Similar reasoning has been used to explain the acceleration in the $H_2$ front typically observed along the length of LNT catalysts during regeneration, i.e., since more $NO_x$ is stored in the front of a given catalyst, more $H_2$ is needed to reduce the stored $NO_x$ and so the front propagates more slowly in this region than in the rear of the catalyst [35]. Additionally, if $NO_x$ is released more slowly from storage sites (due to Pt–Ba phase segregation), such that the kinetics of $NO_x$ reduction are controlled by the rate of $NO_x$ diffusion to the Pt sites, then an acceleration in the velocity of the front edge of the reduction zone is to be expected. Taking these factors together, the increase in selectivity to $NH_3$ can be readily understood.

Evidence for the fact that the kinetics of $NO_x$ reduction in aged catalyst B-225 are not limited by the reductant supply rate is provided by the observation that $NO_x$ release (and hence reduction) is still on-going when $NH_3$ breakthrough occurs at the catalyst outlet. This is illustrated for the degreened and aged B-225 in Fig. 9, which displays the $NO_x$ concentration measured at the 16.4 mm position as a function of time for regeneration events at 200 °C and at 300 °C. The start and end of the regeneration period are indicated, as is the moment when $NH_3$ breakthrough occurs at the 25.4 mm position for the different experiments (note that the data have been time aligned, such that the rich phase starts at the same

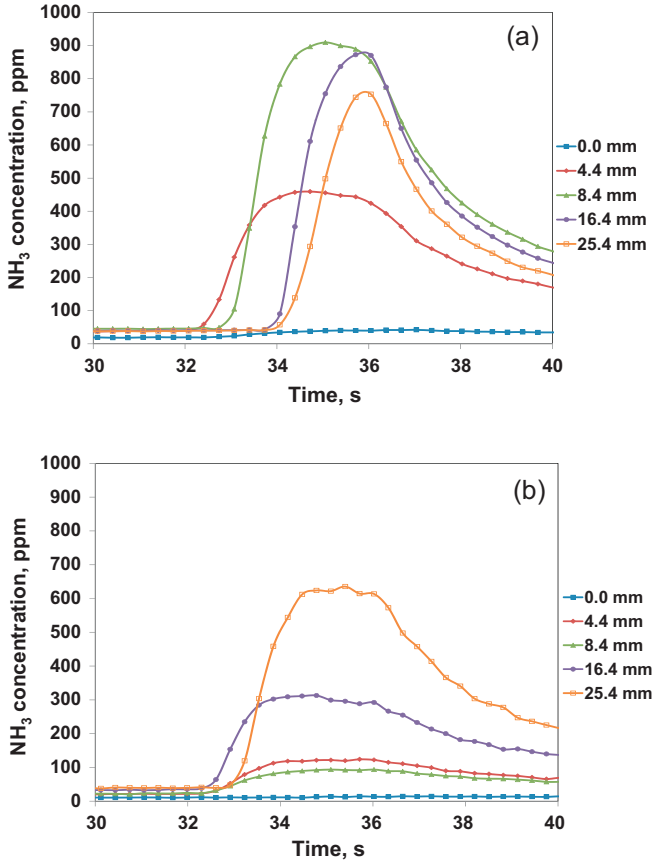


**Fig. 8.** $NH_3$ concentration vs. time at each sampling location at 200 °C for (a) degreened B-225 and (b) aged B-225.

time for each experiment). For degreened B-225 at 200 °C it is evident that some $NO_x$ is still being released at the 16.4 mm position when $NH_3$ breaks through, indicating that at this temperature $NO_x$ reduction is limited by the kinetics of $NO_x$ release, rather than being feed limited. This is in agreement with the report of Clayton et al. [35] cited earlier. For aged B-225 tested at 200 °C, the decrease in the $NH_3$ breakthrough time relative to the degreened catalyst is apparent (corresponding to a shift of ~0.9 s), while it is evident

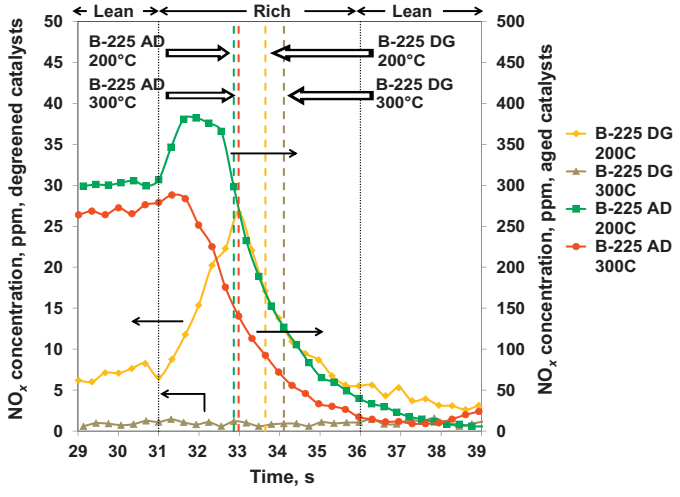


**Fig. 9.** $NO_x$ concentration profiles measured at the 16.4 mm position for degreened (DG) and aged (AD) B-225 as a function of time for regeneration events at 200 °C and at 300 °C. The dashed vertical lines indicate the time at which $NH_3$ breaks through at the 25.4 mm position.

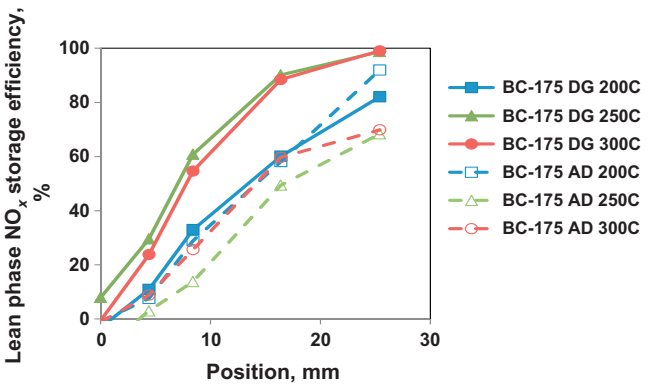


**Fig. 10.** Lean $NO_x$ storage efficiency as a function of position for degreened (DG) and aged (AD) catalyst BC-175.

that considerable $NO_x$ release continues after $NH_3$ breakthrough. In contrast, at 300 °C the degreened catalyst shows essentially no $NO_x$ release at the 16.4 mm position, consistent with fast $NO_x$ release and reduction in the front of the catalyst. However, for the aged catalyst significant $NO_x$ release is observed at 300 °C, while the $NH_3$ breakthrough time is decreased by ~1.2 s. Continued $NO_x$ release after $NH_3$ breakthrough indicates that $NO_x$ reduction, unlike the degreened catalyst, is limited by the kinetics of $NO_x$ release, i.e., even at 300 °C $NO_x$ reduction is not feed limited for the aged catalyst.

### 3.4. Ceria-containing catalyst

#### 3.4.1. NOx storage

As for the experiments with catalyst B-225, cycling experiments using catalyst BC-175 employed a $H_2$ concentration tailored to the OSC and $NO_x$ storage capacity of the catalyst. Fig. 10 reports the measured lean $NO_x$ storage efficiencies. For the degreened catalyst, the NSE increased at each point along the length of the catalyst with increasing temperature. Maximum NSE (<100% at 200 and 250 °C) was not reached until the 25.4 mm position, indicating that the whole length of the catalyst was used for storage under these experimental conditions. Additional information is provided in Fig. 11a and b, in which data pertaining to the cycle-averaged NO and $NO_2$ concentrations are plotted at each measurement point along the length of the catalyst. A gradual decrease in NO concentration along the length of the degreened sample occurs at each temperature with the minimum being attained at the 25.4 mm position.

As with B-225, for BC-175 the $NO_2$ concentration increases along the length of the catalyst for the first third, before decreasing as the rear face of the catalyst is reached. However, it is apparent that $NO_x$ storage is less efficient on BC-175 relative to B-225, as indicated by the longer $NO/NO_2$ storage zone in the case of BC-175. This finding contrast with our previously reported results for similar catalyst compositions in which it was found that the degreened catalysts showed similar NSE at 250 °C under lean–rich cycling conditions [17]. However, in the present study the washcoat loading of BC-175 (175 g/L) was significantly lower than that of B-225 (225 g/L), in contrast to the previous study when the samples used had the same loading. Evidently, NSE under these conditions is sensitive to washcoat loading.

As shown in Table 2, aging of catalyst BC-175 results in the same effects as seen with the non-ceria catalyst, i.e., PGM sintering and hence Pt/Ba and $Pt/CeO_2$ phase segregation. However, comparison of Figs. 2 and 10 indicate that whereas before aging the NSE of B-225 at 200 °C and 250 °C was superior to that of BC-175 (at every position in the catalyst), after aging the NSE of BC-175 is superior to that of B-225. This observation is consistent with our previous

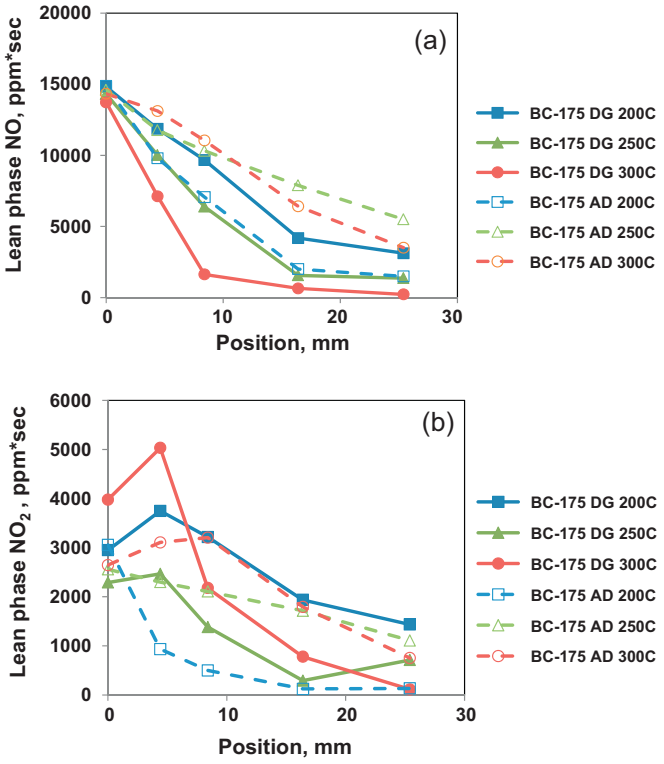


**Fig. 11.** (a) Lean phase NO concentration and (b) lean phase $NO_2$ concentration as a function of position during $NO_x$ storage on degreened (DG) and aged (AD) catalyst BC-175.

studies [16,17,38] indicating the beneficial effects of ceria addition on catalyst performance after aging. Evidently, these benefits more than compensate for the lower washcoat loading of catalyst BC-175 after aging at 800 °C.

### 3.4.2. $NO_x$ reduction

Cycled-averaged $NO_x$ conversion data for the degreened and aged BC-175 samples (see Table 3) are consistent with the NSR zone extending the whole length of the catalyst, the $NO_x$ conversion attaining its maximum value at the rear of the catalyst in each case. Considering the lean phase NSE, while aging results in a decrease in $NO_x$ conversion levels (notably at 300 °C), the deterioration is significantly less than that observed for catalyst B-225 (see Fig. SD2 in the Supplementary Data for a comparison). Again, this serves to illustrate the importance of ceria in aiding LNT durability.

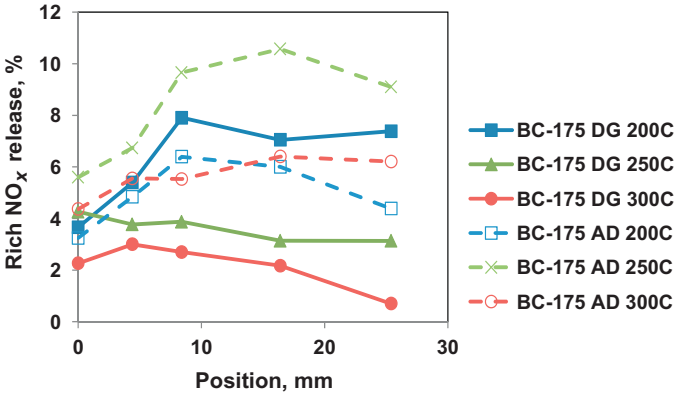


**Fig. 12.** Rich phase $NO_x$ release as a function of position during regeneration of degreened (DG) and aged (AD) catalyst BC-175.

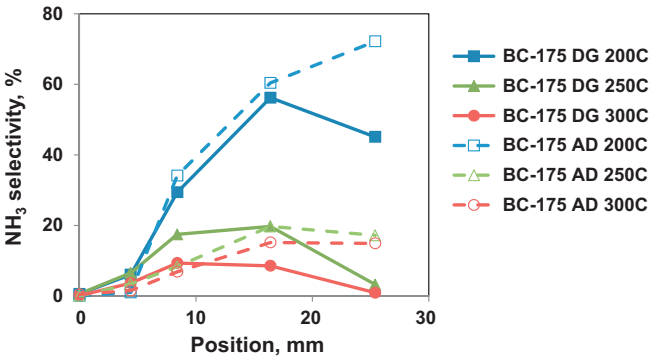


**Fig. 13.** Rich phase $NH_3$ selectivity as a function of position for degreened (DG) and aged (AD) catalyst BC-175.

Fig. 12 depicts the cycle-averaged rich phase $NO_x$ release as a function of measurement position. For the degreened catalyst, the trends in rich phase $NO_x$ release are similar to catalyst B-225, i.e., at 250 and 300 °C $NO_x$ release decreases over the length of the catalyst, indicating that readsorption and reduction of the released $NO_x$ occurs. At 200 °C the $NO_x$ release is notably higher due to the imbalance in the rates of $NO_x$ release and reduction. However, in contrast to B-225, the $NO_x$ release at 200 °C does not decrease significantly in the rear of the BC-175 sample, which can be attributed to the longer $NO_x$ storage–reduction zone in this catalyst.

As for the B-225 catalyst, $NH_3$ formation over BC-175 tracks the $NO_x$ storage zone. Consequently, as shown in Fig. 13, peak $NH_3$ concentrations measured for degreened BC-175 tend to occur closer to the rear of the catalyst in comparison with B-225. Similar to B-225, the selectivity to $NH_3$ exhibited by BC-175 increases after aging. Furthermore, the maxima in $NH_3$ selectivity are located further down the length of the catalyst after aging, consistent with stretching of the NSR zone.

Temporal data for the $NH_3$ release from catalyst BC-175 are shown in Fig. 14a and b. Although not as apparent as with the B-225 catalyst, a delay between the appearance of $NH_3$ for each sampling point is present for the degreened BC-175 catalyst. The fact that the delay is less pronounced than for B-225 can be attributed to the lower washcoat loading of BC-175, and hence the lower concentration of storage sites per unit catalyst length. In contrast to B-225, the $NH_3$ concentration continues to increase down the length of the catalyst. Again, this can be attributed to the lower washcoat of the BC-175 catalyst compared to B-225, which, as discussed earlier, results in utilization of a significantly larger portion of the catalyst for $NO_x$ storage. Since $NH_3$ evolution tracks the $NO_x$ storage–reduction zone, it follows that peak $NH_3$ concentrations for BC-175 are attained further along the catalyst than for B-225. In the case of the aged BC-175 catalyst (Fig. 14b), the delay in $NH_3$ evolution at the different measurement points is again minor, indicative of fast propagation of the reductant front. As for B-225, there is a notable increase in the amount of $NH_3$ released from the aged BC-175 sample after aging. Moreover, similar to B-225, regeneration of BC-175 at 300 °C is limited by the kinetics of $NO_x$ reduction after aging, rather than the rate of reductant supply, as indicated by the observation that $NO_x$ release and reduction is still on-going at the 16.4 mm position when $NH_3$ breaks through the catalyst (see Supplementary Data, Fig. SD3).

As stated in Section 1, there are at least five potential factors which can explain the increase in selectivity to $NH_3$ observed for B-225 and BC-175 after aging. Factor (ii) in the list, pertaining to the decreased OSC of the aged catalysts, and factor (iii) concerning the decrease of the catalyst NSE after aging, were accounted for in this study by adjusting the $H_2$ concentrations used. In this manner, excessively high $H_2$:$NO_x$ ratios in the reductant front were avoided;

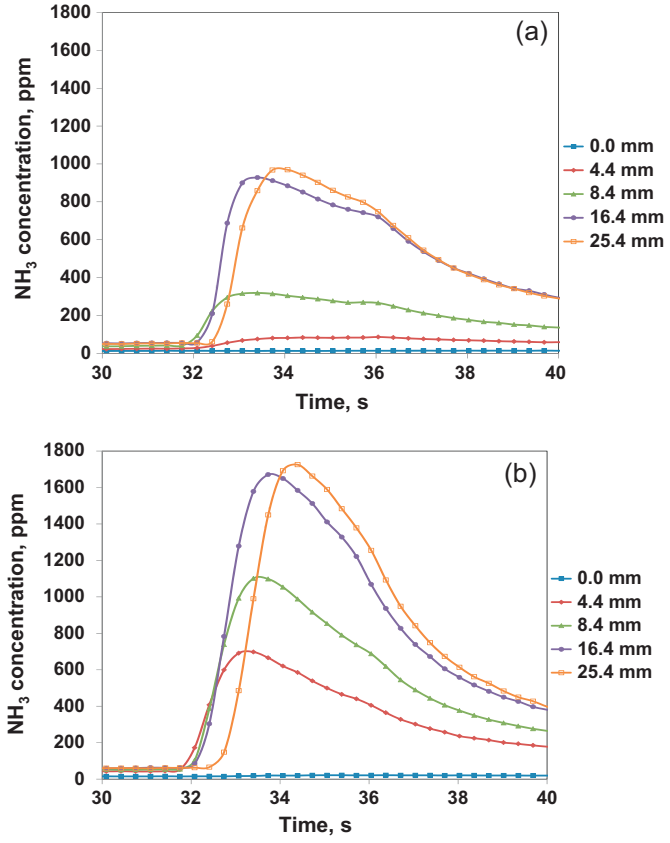


**Fig. 14.** $NH_3$ concentration vs. time at each sampling location at 200 °C for (a) degreened BC-175 and (b) aged BC-175.

instead, a stoichiometric amount of $H_2$ (based on reaction 1) was used during regeneration. With these two factors largely excluded, one or all of the following explanations must be invoked to account for the increase in $NH_3$ selectivity after aging:

(a) The imbalance in the rates of $NO_x$ release and propagation of the reductant front, resulting from the Pt–Ba phase segregation that occurs upon aging. This imbalance results in increased $H_2$:$NO_x$ ratios at the Pt sites, thereby favoring $NH_3$ formation over $N_2$.
(b) Stretching of the NSR zone, resulting from a decrease in concentration of $NO_x$ storage sites per unit length of catalyst. The stretching of this zone decreases the length of the OSC-only zone located in the rear of the catalyst, resulting in diminished $NH_3$ oxidation and decreased $NH_3$ consumption by $NO_x$ that re-adsorbs downstream of the reduction front.
(c) Higher $NH_3$ emissions may result from decreases in the rates of $NH_3$ consumption via reaction with $NO_x$ or $O_2$ stored downstream of the reaction front (due to PGM sintering).

Of these explanations, (a) and (b) are supported by the data presented in this paper. Increased $NH_3$ emissions are clearly associated with stretching of the NSR zone, a conclusion which has previously been reported by workers at Oak Ridge National Laboratory [10–12]. Indeed, as the data in Table 3 show, after aging selectivity to $NH_3$ is most clearly increased at positions towards the end of the catalyst (e.g., at the 16.4 and 25.4 mm positions). At the same time, temporal data show that after aging the rate of reductant front propagation is increased. This, combined with the fact that Pt–Ba phase segregation results in slower transport of $NO_x$ to PGM sites during catalyst regeneration [20], means that $H_2$:$NO_x$ ratios at the PGM sites will increase after aging.

Turning to point (c) above, we have previously presented steady-state, continuous flow data for a catalyst containing the same washcoat composition as B-225 (but slightly higher washcoat loading) [38]. Results showed that after aging (during which the maximum temperature was 770 ± 10 °C) the rate of the $NO_x$-$NH_3$ SCR reaction was measurably decreased. On the other hand, for the same catalyst the kinetics of the $NH_3$-$O_2$ reaction were essentially unchanged [40]. Therefore, in the present work we cannot exclude the possibility that a decrease in the rate of the $NO_x$-$NH_3$ SCR reaction after aging also contributes to the observed increase in catalyst selectivity to $NH_3$.

## 4. Conclusions

SpaciMS was employed in this study to understand the factors influencing the $NH_3$ selectivity of fully formulated LNT catalysts, particularly after thermal aging. Physical characterization of the aged catalysts revealed that the surface area, pore volume and PGM dispersion decreased. This fact helps to explain the decreases in $NO_x$ storage efficiency and increases in $NH_3$ selectivity and rich phase $NO_x$ release observed during lean–rich cycling experiments. Specifically, the losses in surface area, accompanied by segregation of the Pt/Rh sites and BaO storage sites, account for the decreased $NO_x$ storage efficiency of the aged catalysts. During $NO_x$ storage during the lean phase, NO and $NO_2$ were required to travel further to reach storage sites due to the decreased storage site concentration. Consequently, after aging the $NO_x$ storage–reduction zone was elongated.

Stretching of the NSR zone has significant implications for catalyst regeneration. The first effect is the increase of the $NO_x$ "puff" that appears during the onset of the rich front as it travels along the length of the catalyst. Since $NO_x$ release from the catalyst tracks the NSR zone, for an aged catalyst the $NO_x$ concentration peaks closer to the rear of the catalyst. Hence the probability that $NO_x$ can re-adsorb downstream of the reduction front and subsequently undergo reduction by $NH_3$ is diminished, and consequently the $NO_x$ emission is higher.

Second, the "stretching" of the NSR zone causes the $NH_3$ selectivity of an aged catalyst to increase. For degreened (but not aged) catalysts, $NH_3$ is generally observed in the effluent from the catalyst after the stored $NO_x$ and adsorbed oxygen located downstream from its point of generation have been consumed; hence, a longer NSR zone for a given length of catalyst means that less catalyst (corresponding to the OSC-only zone) is available to consume $NH_3$ produced upstream by either the $NH_3$-$NO_x$ SCR or $NH_3$-$O_2$ reaction.

Third, the loss of OSC and $NO_x$ storage sites leads to an increase in the rate of propagation of the reductant front in the aged catalyst compared to the degreened catalyst. Additionally, $NO_x$ is released more slowly from storage sites (due to Pt–Ba phase segregation), such that for the aged catalysts the kinetics of $NO_x$ reduction are controlled by the rate of $NO_x$ diffusion to the Pt sites (rather than being feed limited). Taken together, these factors give rise to increased $H_2$:$NO_x$ ratios at the Pt/Rh sites and hence selectivity to $NH_3$ increases.

## Disclaimer

This report was prepared as an account of work sponsored by an agency of the United States Government. Neither the United States Government nor any agency thereof, nor any of their employees, makes any warranty, express or implied, or assumes any legal liability or responsibility for the accuracy, completeness, or usefulness of any information, apparatus, product, or process disclosed, or represents that its use would not infringe privately owned rights.

References herein to any specific commercial product, process, or service by trade name, trademark, manufacturer, or otherwise does not necessarily constitute or imply its endorsement, recommendation, or favoring by the United States Government or any agency thereof. The views and opinions of authors expressed herein do not necessarily state or reflect those of the United States Government or any agency thereof.

## Acknowledgements

This project was funded by the U.S. Department of Energy (DOE) under award No. DE-EE0000205. The authors also wish to thank Ford Motor Co. for additional funding, provided under the auspices of the Ford University Research Program.

## Appendix A. Supplementary data

Supplementary data associated with this article can be found, in the online version, at http://dx.doi.org/10.1016/j.apcatb.2012.05.002.

## References

[1] L. Xu, R. McCabe, W. Ruona, G. Cavataio, SAE Technical Paper 2009-01-0285 (2009).
[2] R. Zukerman, L. Vradman, M. Herskowitz, E. Liverts, M. Liverts, A. Massner, M. Weibel, J.F. Brilhac, P.G. Blakeman, L.J. Peace, Chemical Engineering Journal 155 (2009) 419.
[3] D. Chatterjee, P. Koči, V. Schmeisser, M. Marek, M. Weibel, B. Krutzsch, Catalysis Today 151 (2010) 395.
[4] P. Forzatti, L. Lietti, Catalysis Today 155 (2010) 131.
[5] A. Lindholm, H. Sjövall, L. Olsson, Applied Catalysis B 98 (2010) 112.
[6] J.-S. Choi, W.P. Partridge, C.S. Daw, Applied Catalysis A 293 (2005) 24.
[7] J.-S. Choi, W.P. Partridge, W.S. Epling, N.W. Currier, T.M. Yonushonis, Catalysis Today 114 (2006) 102.
[8] W.P. Partridge, T.J. Toops, J.B. Green, T.R. Armstrong, Journal of Power Sources 160 (2006) 454.
[9] V.Y. Pridhodko, K. Nguyen, J.-S. Choi, C.S. Daw, Applied Catalysis B 92 (2009) 9.
[10] W.P. Partridge, J.-S. Choi, Applied Catalysis B 91 (2009) 144.
[11] J.-S. Choi, W.P. Partridge, J.A. Pihl, C.S. Daw, Catalysis Today 136 (2008) 173.
[12] J.-S. Choi, W.P. Partridge, C.S. Daw, Applied Catalysis B 77 (2007) 145.
[13] J.-S. Choi, W.P. Partridge, J.A. Pihl, M.-Y. Kim, P. Kočí, C.S. Daw, Catalysis Today 184 (2012) 20.
[14] J.-Y. Luo, M. Al-Harbi, M. Pang, W.S. Epling, Applied Catalysis B 106 (2011) 664.
[15] J. Wang, Y. Ji, V. Easterling, M. Crocker, M. Dearth, R.W. McCabe, Catalysis Today 175 (2011) 83.
[16] Y. Ji, V. Easterling, U. Graham, C. Fisk, M. Crocker, J.-S. Choi, Applied Catalysis B 103 (2011) 413.
[17] Y. Ji, C. Fisk, V. Easterling, U. Graham, A. Poole, M. Crocker, J.-S. Choi, W. Partridge, K. Wilson, Catalysis Today 151 (2010) 362.
[18] Y. Ji, J.-S. Choi, T.J. Toops, M. Crocker, M. Naseri, Catalysis Today 136 (2008) 146.
[19] R.D. Clayton, M.P. Harold, V. Balakotaiah, C.Z. Wan, Applied Catalysis B 90 (2009) 662.
[20] D. Bhatia, M.P. Harold, V. Balakotaiah, Catalysis Today 151 (2010) 314.
[21] V. Perrichon, L. Retailleau, P. Bazin, M. Daturi, J.C. Lavalley, Applied Catalysis 260 (2004).
[22] W. Epling, L. Campbell, A. Yezerets, N. Currier, J. Parks, Catalysis Reviews: Science and Engineering 46 (2004) 163.
[23] I. Nova, L. Lietti, P. Forzatti, Catalysis Today 136 (2008) 128.
[24] D.H. Kim, Y.-H. Chin, G.G. Muntean, A. Yezeretz, N.W. Currier, W.S. Epling, H.-Y. Chen, H. Hess, C.H.F. Peden, Industrial and Engineering Chemistry Research 45 (2006) 8815.
[25] E. Mamontov, T. Egami, R. Brezny, M. Koranne, S. Tyagi, Journal of Physical Chemistry B 104 (2000) 11110.
[26] N. Fekete, R. Kemmler, D. Voigtländer, B. Krutzsch, E. Zimmer, G. Wenninger, W. Strehlau, J.A.A. van den Tillaart, J. Leyrer, E.S. Lox, W. Müller, SAE Technical Paper Series 970746 (1997).
[27] D. Uy, A.E. O'Neill, J. Li, W.L.H Watkins, Topics in Catalysis 95 (2004) 191.
[28] T.J. Toops, B.G. Bunting, K. Nguyen, A. Gopinath, Catalysis Today 123 (2007) 285.
[29] K. Nguyen, H. Kim, B.G. Bunting, T.J. Toops, C.S. Yoon, SAE Technical Paper Series 2007-01-0470 (2007).
[30] M. Casapu, J.-D. Grunwaldt, M. Maciejewski, A. Baiker, S. Eckhoff, U. Göbel, M. Wittrock, Journal of Catalysis 251 (2007) 28.
[31] D.H. Kim, Y.-H. Chin, J.H. Kwak, C.H.F. Peden, Catalysis Letters 124 (2008) 39.
[32] L. Cumaranatunge, S.S. Mulla, A. Yezerets, N.W. Currier, W.N. Delgass, F.H. Ribeiro, Journal of Catalysis 246 (2007) 29.
[33] S.S. Mulla, S.S. Chaugule, A. Yezerets, N.W. Currier, W.N. Delgass, F.H. Ribeiro, Catalysis Today 136 (2008) 136.
[34] L. Letti, I. Nova, P. Forzatti, Journal of Catalysis 257 (2008) 270.
[35] R.D. Clayton, M.P. Harold, V. Balakotaiah, Applied Catalysis B 81 (2008) 161.
[36] J.A. Pihl, J.E. Parks III, C.S. Daw, T.W. Root, SAE Technical Paper Series 2006-01-3441 (2006).
[37] R.D. Clayton, M.P. Harold, V. Balakotaiah, Applied Catalysis B 84 (2008) 616.
[38] J. Wang, Y. Ji, U. Graham, C. Cesar Spindola de Oliveira, M. Crocker, Chinese Journal of Catalysis 32 (2011) 736.
[39] A. Martínez-Arias, M. Fernández-García, A. Iglesias-Juez, A.B. Hungria, J.A. Anderson, J.C. Conesa, J. Soria, Applied Catalysis B 38 (2002) 151.
[40] J. Wang, M. Crocker, unpublished results.